Research Article | Vol. 31, No. 6 / 13 Mar 2023 / Optics Express 10541
Optics EXPRESS

Simulated depolarization ratios for dust and smoke at laser wavelengths: implications for lidar application

ZHONGWEI HUANG,[1,2] XINGTAI SHEN,[1] SHIHAN TANG,[1] TIAN ZHOU,[1,*] QINGQING DONG,[1] SHUANG ZHANG,[1] MEISHI LI,[1] AND YONGKAI WANG[1]

[1]*Key Laboratory for Semi-Arid Climate Change of the Ministry of Education, College of Atmospheric Sciences, Lanzhou University, Lanzhou 730000, China*
[2]*Collaborative Innovation Center for West Ecological Safety (CIWES), Lanzhou University, Lanzhou 730000, China*
[*]*zhoutian@lzu.edu.cn*

Abstract: Polarization measurements have been widely used to detect aerosol properties by remote sensing in recent decades. To better understand the polarization characteristics of aerosols by lidar, the numerically exact T-matrix method was used to simulate the depolarization ratio (DR) of dust and smoke aerosols at typical laser wavelengths in this study. The results show that the DRs of dust and smoke aerosols have obviously different spectral dependences. Moreover, the ratio of DRs at two wavelengths has an obvious linear relationship with the microphysical properties of aerosols, including aspect ratio, effective radius and complex refractive index. At short wavelengths, we can use it to invert the absorption characteristics of particles, further improving the detection ability of lidar. Comparing the simulation results of different channels, DR, (color ratio) CR and (lidar ratio) LR have a good logarithmic fitting relationship at 532 nm and 1064 nm, which helps to classify the aerosol types. On this basis, a new inversion algorithm, "1β+1α+2δ", was presented. By this algorithm, the backscattering coefficient (β), extinction coefficient (α), DR (δ) at 532 nm and 1064 nm can be used to expand the range of inversion and compare lidar data with different configurations to obtain more extensive optical characteristics of aerosols. Our study enhances the application of laser remote sensing in aerosol observations more accurately.

1. Introduction

Atmospheric aerosols play a key role in the Earth's climate system and directly affect the radiation budget by scattering and absorbing solar and terrestrial radiation or indirectly affect it by forming cloud condensation nuclei or ice nuclei [1–5]. In addition, aerosols can also affect the human respiratory system, leading to respiratory diseases and even cancer [6]. Therefore, the detection of aerosol radiation characteristics is crucial to the study of climate change and environmental governance. The radiation characteristics of aerosols depend on their morphological structure and chemical components, while in reality, aerosol particles have irregular morphological structures and complex chemical components [7,8]. For example, the shape of dust aerosols is often cylindrical, ellipsoidal, etc., and sulfate and other substances are often attached, which makes it difficult to accurately observe their radiation characteristics [9,10]. Therefore, confirmation of the aerosol type is very useful for accurate calculation of the aerosol radiative forcing and its related impacts.

Polarization lidar is an important tool for remote sensing that can provide vertically resolved information on aerosol optical properties [11–14]. The backscattering information received by lidar, such as the depolarization ratio (DR), lidar ratio (LR), and color ratio (CR), can be used to

#484335 https://doi.org/10.1364/OE.484335
Journal © 2023 Received 26 Dec 2022; revised 8 Feb 2023; accepted 21 Feb 2023; published 8 Mar 2023

Optics EXPRESS

classify aerosols and retrieve their microphysical properties [15,16]. DR is defined by the ratio of perpendicular to parallel backscattering intensity with respect to the polarization plane of the emitted laser, and it is an important parameter to measure the particles' nonsphericity [17]. The microphysical properties of aerosols, including particle size distribution and complex refractive index, also have a great impact on DR [18]. Thus, DR is used to classify aerosol type and to invert the effective radius and mass concentration of particles [19,20]. In particular, Huang et al. [21] found that the spectral dependence of DR has a good fitting relationship with its absorption coefficient.

At present, the T-matrix method is one of the most widely used methods to simulate aerosol optical properties with high accuracy [22]. Mishchenko et al. [23] analyzed measurements of the backscattering linear depolarization ratio (LDR) for a plume of aged smoke at lidar wavelengths ranging from 355 to 1064 nm by using the numerically exact (superposition) T-matrix method. Bi et al. [24] investigated the optical properties of sea salt aerosols using invariant imbedding T-matrix simulations and proved the dependence of the LDR of sea salt aerosols on relative humidity. Information on LDR at laser wavelengths for dust and smoke is important for accurately detecting aerosol properties by lidar. Thus, in this study, the T-matrix method was used to simulate the spectral dependence of aerosols and further investigate the relationship between DR and other aerosol properties, aiming to optimize the polarization channels of aerosol lidar. In addition, the widely used ellipsoidal model was mainly used to simulate the morphological structure of dust and smoke [25,26].

The main purpose of this study is to further improve the detection ability of polarized lidar by providing important information for lidar development and retrieval methods. Simulating the relationship between aerosol optical properties and microphysical properties provides an important theoretical basis. In Section 2, the optical and microphysical properties of aerosols used in this simulation process are briefly introduced. In Section 3, the spectral dependence of DR for dust and smoke is verified. Then, the correlation between optical parameters and microphysical properties was investigated. Finally, a new recognition algorithm is proposed. Section 4 summarizes this study.

2. Method

2.1. Definition of optical parameters

The depolarization ratio (DR or δ) of aerosols is related not only to their shape but also to the wavelength of incident light, spatial orientation, size distribution, complex refractive index and other factors [27,28]. It is assumed in this work that aerosol particles are homogeneous and randomly oriented, the incident light is horizontally polarized, and the size distribution is lognormal. Only the effects of the effective radius (R_{eff}), complex refractive index (M) and aspect ratio (AR) were considered.

The incident and scattered light of particles can be expressed by Stokes parameters as $(I_0, Q_0, U_0, V_0)^T$ and $(I, Q, U, V)^T$, where T means transpose of given array. When the incident light is horizontally polarized, $(I_0, Q_0, U_0, V_0)^T=(1, 1, 0, 0)^T$ [29]. For the Stokes parameters, $I = I_{//} + I_\perp$ and $Q = I_{//} - I_\perp$, where $I_{//}$ and $I_\perp$ denote the intensity of scattered light parallel and vertical to the scattering plane, respectively. $I_\perp$ and $I_{//}$ of the scattered light in the backscattering direction are expressed as $I_\perp(\pi)$ and $I_\parallel(\pi)$, so δ can be expressed as:

$$\delta = I_\perp(\pi)/I_\parallel(\pi) \tag{1}$$

Optics EXPRESS

The elements of the normalized 4×4 Stokes scattering matrix have the following well-known structure [30]:

$$\begin{pmatrix} I \\ Q \\ U \\ V \end{pmatrix} \propto \begin{pmatrix} a_1(\pi) & 0 & 0 & 0 \\ 0 & a_2(\pi) & 0 & 0 \\ 0 & 0 & a_3(\pi) & 0 \\ 0 & 0 & 0 & a_4(\pi) \end{pmatrix} \begin{pmatrix} 1 \\ 1 \\ 0 \\ 0 \end{pmatrix} \tag{2}$$

where the (1, 1) element of scattering matrix, $a_1(\pi)$, is the conventional phase function; and π is the scattering angle. Combining Eq. (1) and Eq. (2), δ is defined by:

$$\delta = \frac{a_1(\pi) - a_2(\pi)}{a_1(\pi) + a_2(\pi)} \tag{3}$$

Only one parameter of DR has difficulty in accurately classifying aerosol type, so other parameters need to be used. Using the T-matrix method, we can not only obtain the DR of particles but also obtain the CR and LR. CR reflects the size of particles, and LR reflects the direction characteristics of light scattering of particles [31]. There is a certain correlation between different optical parameters, and we can classify aerosol types according to this conclusion [32,33]. For an individual particle, CR and LR can be calculated by the following equation [34]:

$$CR(\lambda_1, \lambda_2) = \frac{a_1(\pi, \lambda_1) C_{sca}(\lambda_1)}{a_1(\pi, \lambda_2) C_{sca}(\lambda_2)} \tag{4}$$

$$LR(\lambda_1) = \frac{4\pi C_{ext}(\lambda_1)}{a_1(\pi, \lambda_1) C_{sca}(\lambda_1)} \tag{5}$$

where C_{ext} and C_{sca} are the extinction cross section and scattering cross section of particles, respectively, λ_1 and λ_2 represent the wavelengths of different lidar channels, and $\lambda_1 > \lambda_2$.

2.2. Microphysical parameters

2.2.1. Wavelength (λ)

The four most commonly used channels are selected, which are 266 nm, 355 nm, 532 nm and 1064 nm. At present, the polarization channels are mostly 355 nm and 532 nm, while the polarization channels of 1064 nm are seldom used due to the high excitation energy. However, observations show that DR data at the 1064 nm channel can further identify aerosol types and improve inversion accuracy [35].

2.2.2. Shape

The spectral dependence of simple ellipsoidal particles is modeled to represent that of nonspherical aerosols that is characterized by the aspect ratio (AR). AR is defined as the ratio of the major axis to the minor axis of the ellipsoid. When AR = 1, the particle is a regular sphere. The AR of dust is the range of 1.20-1.60 [36–40], and the step length is 0.04. The shape and structure of smoke are more complex than those of dust. At present, the fractal model was used to simulate smoke in most studies [41]. However, it is convenient to compare the simulation results of smoke and dust by using the ellipsoidal model. The simulation results of Gialitaki et al. [42] show that the near-spherical smoke model is still consistent with the observation results. The AR of smoke is the range of 0.80-1.20 [23,42,43], and the step length is 0.04.

2.2.3. Effective radius (R_{eff})

Due to the calculation accuracy of the T-matrix method, the size of particles is limited to a certain extent. Dust R_{eff} ranges from 0.2 to 2.4 μm and smoke R_{eff} ranges from 0.1-1.0 μm [23,37,41–43].

Optics EXPRESS

2.2.4. Complex refractive index (M)

The complex refractive index, M = MR + MI, reflects the chemical composition of aerosols, where MR is the real part of M and MI is the imaginary part of M. Since MR has slight variations with the wavelength [44], in this study, the impact of MR is not considered, and the MR of dust and smoke are set as constant values of 1.53 and 1.45, respectively. The MI of dust is set as 0.002-0.020, and the MI of smoke is set as 0.005-0.050 [39,40,42] (all parameters are shown in Table 1).

3. Results and discussion

3.1. Spectral dependence of DR

Burdon et al. [45] analyzed DR data from the NASA Langley airborne High Spectral Resolution Lidar-2 (HSRL-2) and noted that there is not a single consistent spectral dependence of DR. Zo et al. [46] found that the spectral variation in DR differed according to the aerosol type. To verify these conclusions, we simulated the effects of AR and R_{eff} on the DR spectra of dust and smoke under different MIs in this section. It is worth mentioning that the simulation range of dust and smoke MI was not consistent. First, the selection of MI refers to the absorption characteristics in actual observations. Second, the impact of aerosol mixing was not considered in this study.

The simulated dust DR in Fig. 1 ranges from 0.064 to 0.391, which is basically consistent with the long-term observations of the Asian dust DR [47,48]. The DR spectrum shows a trend of first increasing and then decreasing, which is also consistent with the observed results of Burdon et al. [45] Fig. 1(a)–1(c) shows the impact of AR on dust. It is not difficult to find that AR and DR do not always show a monotonic increasing relationship. For example, in Fig. 1(c), even DR decreases with increasing AR at 266 nm and 355 nm. In fact, there is a large error in identifying aerosol types only by DR at a single wavelength, which is one of the reasons why this study is devoted to discussing depolarization ratio spectra. Figure 1(d)–1(f) shows the effect of R_{eff}. The influence of R_{eff} varies greatly at different wavelengths. Dust DR is not sensitive to changes in R_{eff} at 355 nm and 1064 nm. Only at 532 nm, dust DR and R_{eff} have obvious positive correlation. The results show that for the detection of different types of aerosols, the longer or shorter wavelength is not the better. Finally, we found that MI mainly affects DR at short wavelengths.

Compared with dust, smoke DR shows great differences in range and spectral properties. The range of smoke DR is 0.001-0.773, and the spectrum has a decreasing trend. The reasons for such a huge difference are not only the morphological structure but also the chemical composition, that is, the complex refractive index. It can be seen from Fig. 2(a)–2(c) that the greater the nonsphericity is, the greater the smoke DR. This is also in line with the simulated results from Bi et al. [49], that is, the DR of the near-sphere model basically shows a monotonic increasing trend with nonsphericity. When MI = 0.005 or 0.02, There is no obvious change in smoke DR with the same R_{eff}. At different wavelengths, R_{eff} is positively correlated with smoke DR. But when MI = 0.05, smoke DR of large R_{eff} has changed significantly. Figure 2(f) shows the great impact of MI on the DR spectrum. Smoke DR drops to approximately 0.162-0.268 at the short band, and the spectrum also changes greatly, showing a trend of first increasing and then decreasing, which is consistent with Zo et al. [46]

3.2. Ratio of DRs

The following conclusions can be drawn from the simulated results in Section 3.1: the DRs of aerosols have different spectral dependences and are affected by physical properties such as R_{eff}, AR and MI. This conclusion shows that the spectral properties of DR can help classify aerosol types and retrieve physical properties, which further explores the application potential of DR. [50] We define a parameter, the ratio of depolarization ratios (RDR), to reflect the spectral

Optics EXPRESS

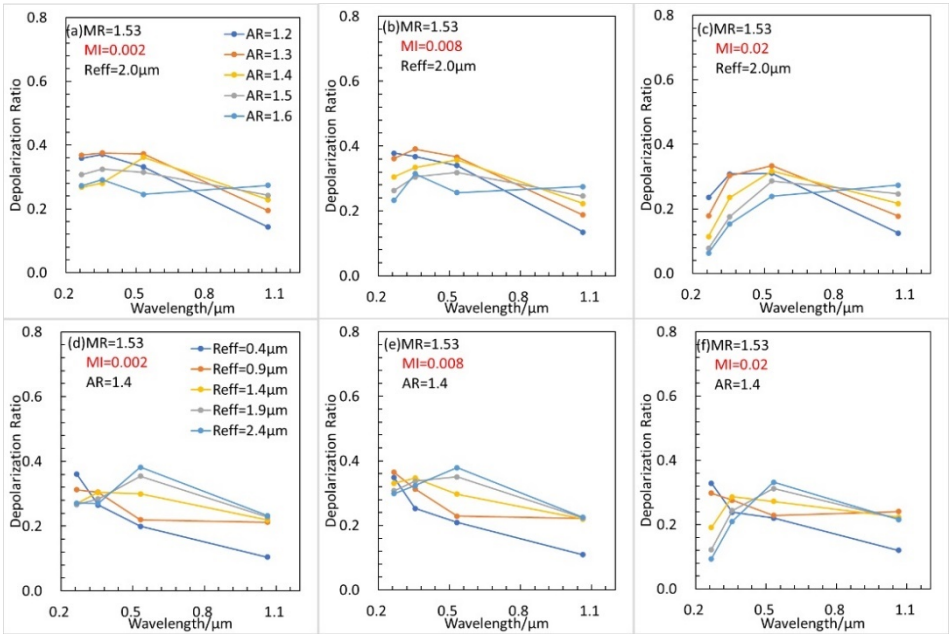

Fig. 1. The effects of microphysical parameters on the depolarization ratio of dust aerosols at 0.266 μm, 0.355 μm, 0.532 μm, and 1.064 μm; (a)-(c) aspect ratio; (d)-(f) effective radius.

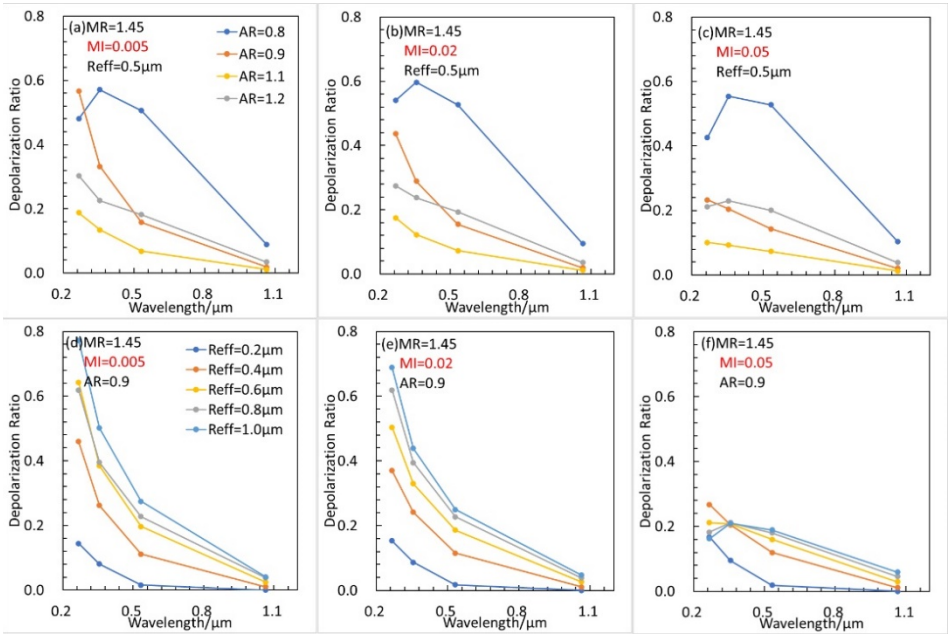

Fig. 2. Same as Fig. 1 but for smoke aerosol.

Optics EXPRESS

properties of DR and discuss the impact of aerosol microphysical characteristics on the parameter. RDR=δ_1/δ_2, where δ_1 and δ_2 are DRs at wavelengths λ_1 and λ_2 ($\lambda_1>\lambda_2$), respectively.

In Fig. 3(a)–3(c), there are not exactly good linear correlation between three microphysical parameters and RDR(Dust), however, it still shows some application prospects of RDR. First, RDR does not cover up the nonsphericity of particles. The relationships among $RDR_{1064/266}$, $RDR_{1064}/_{355}$, $RDR_{1064}/_{532}$ and AR are more linear than those of DR in a single band. Second, in the actual observation of dust, it is rare to see such a large span of absorption characteristics, as shown in Fig. 3(c). Huang et al. [21] found that $RDR_{532}/_{355}$ has a good fitting relationship with the absorption coefficient. The smoke situation is shown in Fig. 3(d)–3(f). Different from dust, although RDR(Smoke) and microphysical properties have good linear correlations, the values and rates of $RDR_{1064}/_{266}$, $RDR_{1064}/_{355}$ and $RDR_{1064}/_{532}$ decrease. Comparing dust with smoke, $RDR_{1064}/_{355}$ and $RDR_{1064}/_{532}$ are quite different from aerosol types, but for the same type, there is only little difference between them. This shows that we can choose one of them as a parameter to identify aerosol types. Considering that the polarization channel at 532 nm is more widely used at present, we suggest choosing $RDR_{1064}/_{532}$. $RDR_{532}/_{355}$ has a better rate of change, which should be more suitable for inverting microphysical properties in a single aerosol environment.

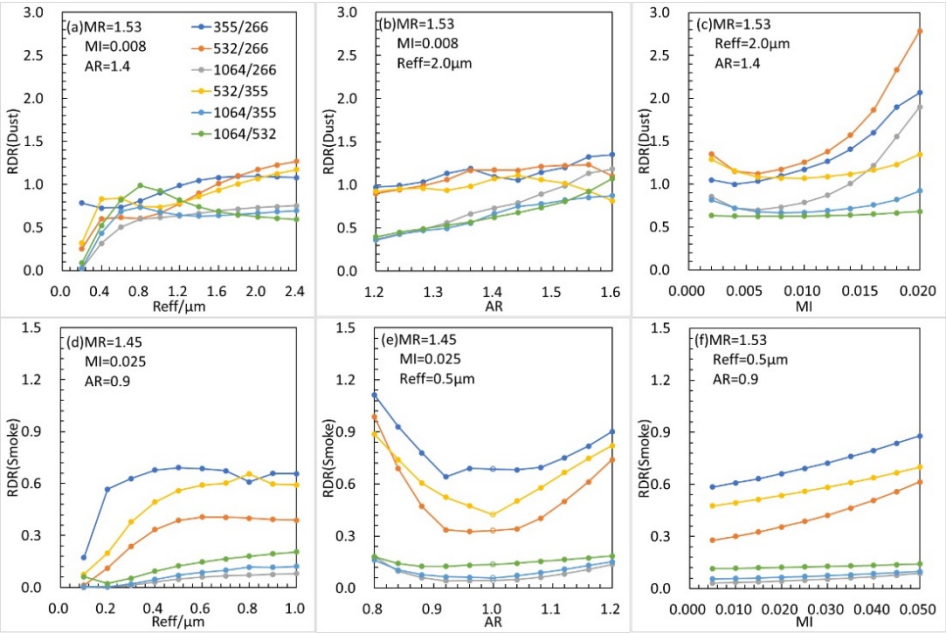

Fig. 3. The effects of microphysical parameters on RDR of aerosol types; (a-c) Dust aerosols; (d-f) Smoke aerosols.

3.3. Relevant optical parameters

In addition to DR, CR and LR are also important parameters for identifying aerosol types. Bi et al. [51] simulated the sensitivity of CR to ice particle habits at wavelengths of 532 nm and 1064 nm. It is proven that the relationship between CR and R_{eff} is affected by aerosol types. Haarig et al. [52] measured DR and LR of aged smoke particles at 355 nm, 532 nm and 1064 nm and found that spectral dependence of LR is different from that of DR.

Optics EXPRESS

3.3.1. Color ratio (CR)

Figures 4,5 show the impact of microphysical properties on CR and LR at 266 nm, 355 nm, 532 nm and 1064 nm, respectively, and the parameters used for simulation are consistent with Fig. 3. It can be seen from Fig. 4 that the dust CR is concentrated at approximately 1.5-4.2, while the value at $CR_{1064/266}$ is even greater than 6.0. This phenomenon is due to the large difference between the scale parameters of dust at 266 nm and 1064 nm, resulting in a huge difference in the backscattering cross section. For data greater than 6.0, considering the actual observation range of CR, we regard it as the error of the algorithm. Smoke CR is concentrated in the range of 0.3-1.8, which is obviously different from that of dust, which proves the importance of CR in identifying aerosol types.

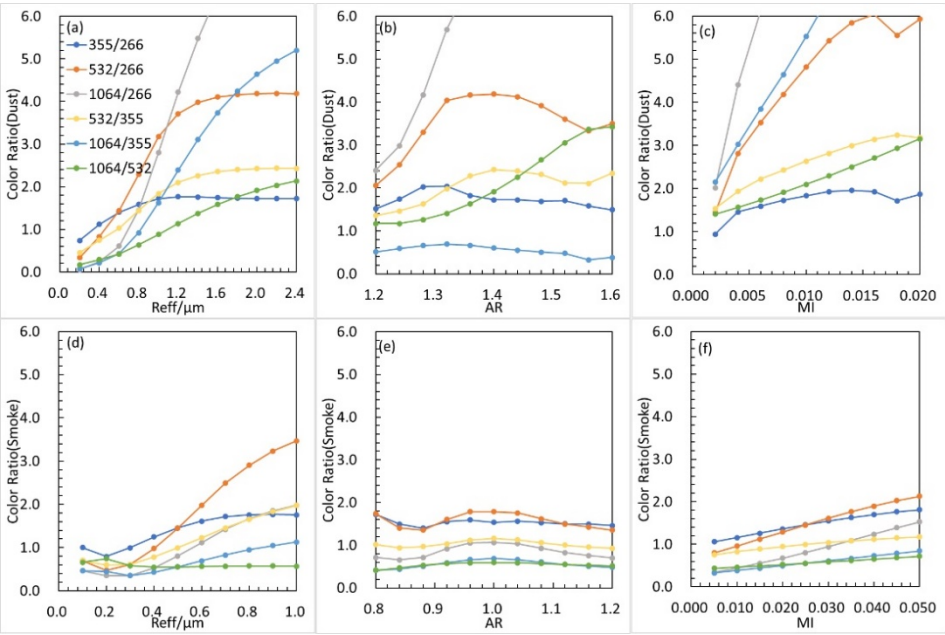

Fig. 4. The effects of microphysical parameters on CR; (a-c) Dust aerosols; (d-f) Smoke aerosols.

3.3.2. Lidar ratio (LR)

Figure 5 shows the variation in dust and smoke LRs with microphysical properties. Dust LR is obviously affected by the microphysical properties at 266 nm, which is basically a positive correlation. With increasing wavelength, the rate of change gradually decreases, and LR at 1064 nm is basically kept at 10-30 sr except for the law of sharp decrease when R_{eff} is small. The variation rule of dust LR at 532 nm in Fig. 5(a) also explains why the LR measured by Shen et al. [53] decreases sharply with decreasing height. It is precisely the impact of large size dust transported by dust storms from northwest China. The change rule of smoke LR with wavelength is contrary to that of dust, showing a positive correlation, which is consistent with the observation results of Haarig et al. [52]

3.4. Recognition algorithm

Summarizing the previous simulation results, we find that for different types of aerosols, their optical properties are obviously different, especially in spectral dependence. Using two or

Optics EXPRESS

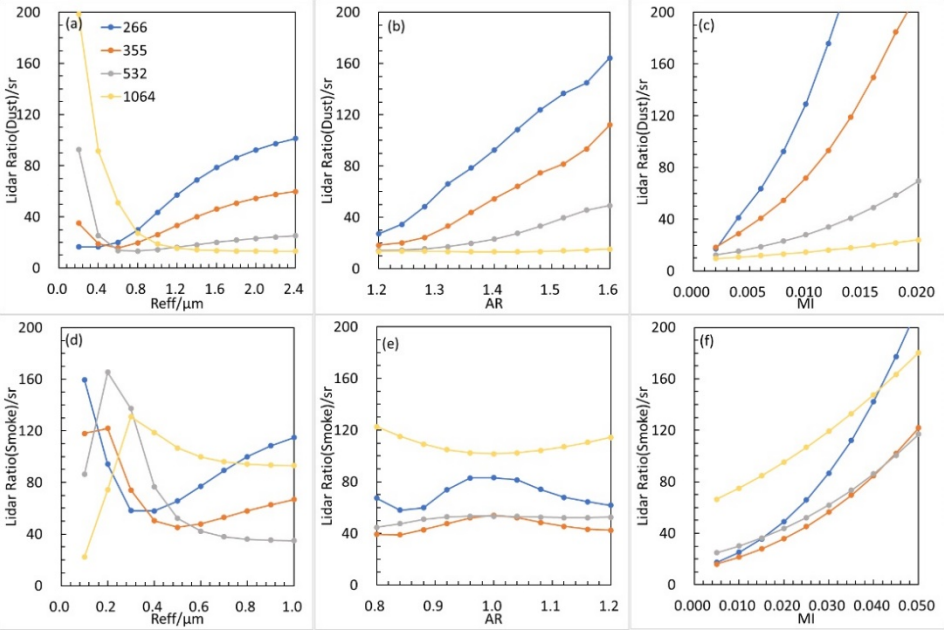

Fig. 5. The effects of microphysical parameters on LR; (a-c) Dust aerosols; (d-f) Smoke aerosols.

more optical parameters at different wavelengths to identify aerosol types and retrieve physical parameters are also mainstream methods at present, such as "3β+2α+1δ" and "2β+1δ" [54,55], where β is the backscattering coefficient and α is the extinction coefficient. We hope to develop a new identification method that can achieve the following purposes: (1) The algorithm can be adapt to different conditions: the long-distance transportation of a single aerosol type or the aerosol identification of a complex environment; and (2) the lidar channels can be reduced as much as possible. The second point is convenient to compare lidar data of different configurations to obtain more extensive physical properties of aerosols.

Figure 6 shows the RDR fitting relationship between CR and the ratio of LRs and their classified effects on dust and smoke, where the red dot represents the observed data from references in Table 2 and 3. We can draw two main conclusions: (1) In general, the classified effect at 1064 nm is more significant, which also conforms to our conclusion in Section 3.2.2; (2) From the simulated results, there is a good fitting relationship with RDR and the other two parameters except 355/266, but the data in references are obviously different from the simulated results except for Fig. 6(l). This is because the aerosol model is different from the actual particles, the error of the algorithm itself, and the sample size is too small. These points prove that the backscatter data at long wavelengths are more conducive to classifying aerosol types. The effect of 1064 nm and 532 nm is better than that of 532 nm and 355 nm, both from the fitting relationship between lidar parameters and the classification effect between different models. Based on the above simulated results and Eq. (4),(5), LR and CR at 532 nm or 1064 nm can be obtained through the remaining Lidar data at these two channels. And we propose a new recognition algorithm: "1β+1α+2δ". This means that the backscattering coefficient, extinction coefficient, depolarization ratio at 532 nm and depolarization ratio at 1064 nm are used for aerosol identification and physical property inversion. The application of the new recognition algorithm at 355 nm and 266 nm requires the improvement of the aerosol model and the feedback of more observed data.

Optics EXPRESS

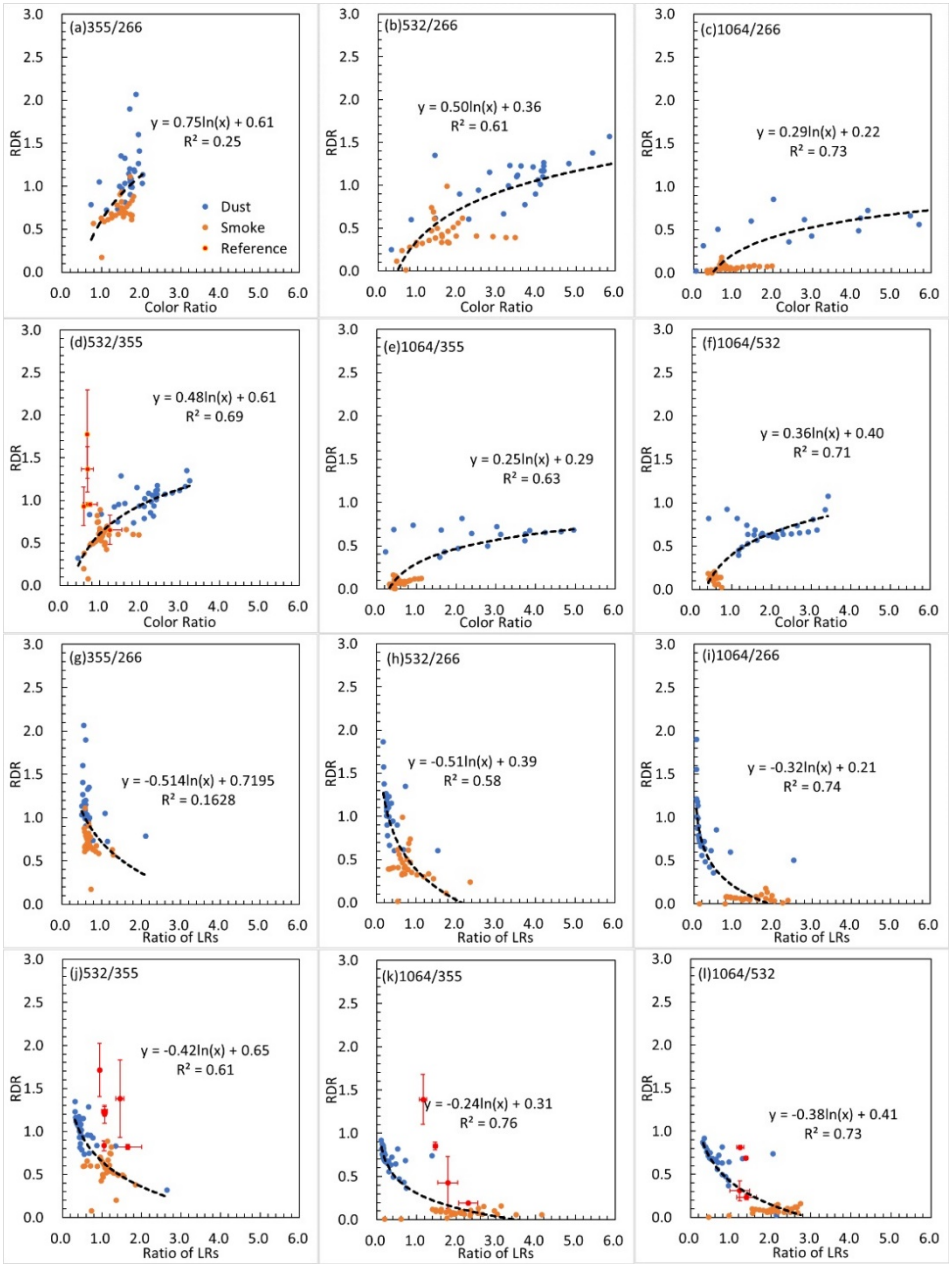

Fig. 6. The effects of microphysical parameters on RDR of aerosol types; (a-f) Color Ratio; (g-l) The ratio of Lidar ratios.

Optics EXPRESS

Table 1. The parameters of the dust and smoke models

	Dust aerosol	Smoke aerosol
λ/nm	266, 355, 532, 1064	
AR	1.20, 1.24, 1.28, 1.32, 1.36, 1.40, 1.44, 1.48, 1.52, 1.56, 1.60	0.80, 0.84, 0.88, 0.92, 0.96, 1.00, 1.04, 1.08, 1.20
R_{eff}/μm	0.2, 0.4, 0.6, 0.8, 1.0, 1.2, 1.4, 1.6, 1.8, 2.0, 2.2, 2.4	0.1, 0.2, 0.3, 0.4, 0.5, 0.6, 0.7, 0.8, 0.9, 1.0
MR	1.53	1.45
MI	0.002, 0.004, 0.006, 0.008, 0.010, 0.012, 0.014, 0.016, 0.018, 0.020	0.005, 0.010, 0.015, 0.020, 0.025, 0.030, 0.035, 0.040, 0.045, 0.050

Table 2. Depolarization ratio and backscattering coefficient in Ref. [56]

PDR 355	PDR 532	Backscatter coefficient 355/($Mm^{-1}sr^{-1}$)	Backscatter coefficient 532/($Mm^{-1}sr^{-1}$)
0.08 ± 0.03	0.10 ± 0.03	0.44 ± 0.15	0.27 ± 0.08
0.09 ± 0.03	0.16 ± 0.10	0.38 ± 0.09	0.26 ± 0.06
0.11 ± 0.03	0.15 ± 0.07	0.48 ± 0.14	0.33 ± 0.17
0.10 ± 0.02	0.38 ± 0.23	0.99 ± 0.47	1.27 ± 0.86
0.14 ± 0.03	0.13 ± 0.06	0.44 ± 0.12	0.26 ± 0.07
0.20 ± 0.11	0.19 ± 0.10	0.40 ± 0.06	0.28 ± 0.05
0.22 ± 0.11	0.21 ± 0.10	0.62 ± 0.16	0.47 ± 0.23
0.46 ± 0.26	0.30 ± 0.09	1.01 ± 0.44	1.26 ± 0.85

Table 3. Depolarization ratio and lidar ratio in references

Reference	Lidar Ratio/sr			Depolarization Ratio		
	355 nm	532 nm	1064 nm	355 nm	532 nm	1064 nm
Groß et al. (2011) [57]	58 ± 7	62 ± 5	-	0.25 ± 0.03	0.30 ± 0.01	-
Groß et al. (2015) [58]	53 ± 5	56 ± 7	-	0.26 ± 0.03	0.217 ± 0.01	-
Haarig et al. (2018) [52]	46 ± 6	67 ± 4	82 ± 22	0.021 ± 0.040	0.029 ± 0.015	0.009 ± 0.008
	40 ± 16	66 ± 12	92 ± 27	0.224 ± 0.015	0.184 ± 0.006	0.043 ± 0.007
Haarig et al. (2022) [59]	47 ± 8	50 ± 5	69 ± 14	0.242 ± 0.024	0.299 ± 0.018	0.206 ± 0.01
	49 ± 4	46 ± 5	57 ± 9	0.174 ± 0.041	0.298 ± 0.016	0.242 ± 0.007

4. Conclusion

In this study, the T-matrix method is used to simulate the linear depolarization ratio (LDR) spectra of dust aerosols and smoke aerosols with random orientation and lognormal distribution, and the impact of different microphysical parameters on LDR is discussed. The simulated results show that DR has obvious spectral dependence, and the ratio of DRs can be used to represent the property. In general, researchers use DR to classify aerosol types by the threshold method. In this study, we can also use the same method to exploit RDR. The RDR value of 1.0 could be used as a threshold for distinguishing dust and smoke aerosols at 532 nm and 355 nm. Moreover, we found that RDR has a good fitting relationship with the absorption coefficient, especially at low wavelengths. This conclusion confirms the potential inversion ability of RDR.

Combining the simulation of CR and LR, we finally established suitable detection channels for lidar. High band channels, 1064 nm and 532 nm, are more suitable for identifying aerosol types, and low band channels should be used when retrieving parameters of a single aerosol type. For example, 1064 nm and 355 nm are suitable for retrieving dust aerosols, while 532 nm and

Optics EXPRESS

355 nm are more suitable for retrieving smoke aerosols. We further propose a new recognition method: "1β+1α+2δ". By comparing the data in references, we can verify that the recognition algorithm has a considerable degree of feasibility, but there are still the following shortcomings to be improved: (1) the number of aerosol models used is small, which cannot be adapt to more complex situations, such as the identification and inversion of pollution dust particles and sea salt particles; (2) the inversion of microphysical properties lacks quantitative analysis; and (3) there is still a certain error between the simulated value and the observed value. In fact, the purpose of the algorithm is to expand the retrieval data of lidar and facilitate the comparison of lidar data with different configurations. It is more suitable for a case with fewer lidar channels.

Funding. Gansu Provincial Science and Technology Innovative Talent Program: High-level Talent and Innovative Team Special Project (No.22JR9KA001); the Second Tibetan Plateau Scientific Expedition and Research Program (Grant No. 2019QZKK0602); National Natural Science Foundation of China (41975019); 111 Project (B 13045); Fundamental Research Funds for the Central Universities (lzujbky-2022-kb10, lzujbky-2022-kb11).

Acknowledgments. Thanks for the T-matrix code provided by Prof. M. I. Mishchenko (http://www.giss.nasa.gov/staff/mmishchenko/t_matrix.html).

Disclosures. The authors declare no conflicts of interest.

Data availability. Data underlying the results presented in this paper are not publicly available at this time but may be obtained from the authors upon reasonable request.

References

1. D. Rosenfeld, M. O. Andreae, A. Asmi, M. Chin, G. Leeuw, D. P. Donovan, R. Kahn, S. Kinne, N. Kivekäs, M. Kulmala, W. Lau, K. Sebastian Schmidt, T. Suni, T. Wagner, M. Wild, and J. Quaas, "Global observations of aerosol-cloud-precipitation-climate interactions," Rev. Geophys. **52**(4), 750–808 (2014).
2. U. Lohmann and J. Feichter, "Global indirect aerosol effects: a review," Atmos. Chem. Phys. **5**(3), 715–737 (2005).
3. R. J. Charlson, J. Langner, H. Rodhe, C. B. Leovy, and S. G. Warren, "Perturbation of the Northern Hemisphere radiative balance by backscattering from anthropogenic sulfate aerosols," Tellus A **43**(4), 152–163 (1991).
4. T. Deshler, "A review of global stratospheric aerosol: Measurements, importance, life cycle, and local stratospheric aerosol," Atmos. Res. **90**(2-4), 223–232 (2008).
5. Z. Huang, J. Huang, T. Hayasaka, S. Wang, T. Zhou, and H. Jin, "Short-cut transport path for Asian dust directly to the Arctic: A case study," Environ. Res. Lett. **10**(11), 114018 (2015).
6. G. Oberdörster, Z Sharp, V Atudorei, A. Elder, R. Gelein, W. Kreyling, and C. Cox, "Translocation of inhaled ultrafine particles to the brain," Inhalation Toxicol. **16**(6-7), 437–445 (2004).
7. S. Merikallio, H. Lindqvist, T. Nousiainen, and M. Kahnert, "Modelling light scattering by mineral dust using spheroids: Assessment of applicability," Atmos. Chem. Phys. **11**(11), 5347–5363 (2011).
8. K. Kandler, K. Lieke, N. Benker, C. Emmel, M. Küpper, D. Müller-Ebert, M. Ebert, D. Scheuvens, A. Schladitz, L. Schütz, and S. Weinbruch, "Electron microscopy of particles collected at Praia, Cape Verde, during the Saharan Mineral Dust Experiment: Particle chemistry, shape, mixing state and complex refractive index," Tellus B **63**(4), 475–496 (2011).
9. J. Helmert, B. Heinold, I. Tegen, O. Hellmuth, and M. Wendisch, "On the direct and semidirect effects of Saharan dust over Europe: A modeling study," J. Geophys. Res. **112**(D13), 2006JD007444 (2007).
10. A. Ansmann, A. Petzold, K. Kandler, I. Tegen, M. Wendisch, D. Müller, B. Weinzierl, T. Müller, and J. Heintzenberg, "Saharan Mineral Dust Experiments SAMUM-1 and SAMUM-2: What have we learned?" Tellus B Chem Phys Meteorol **63**(4), 403–429 (2011).
11. T. Murayama, H. Okamoto, N. Kaneyasu, H. Kamataki, and K. Miura, "Application of lidar depolarization measurement in the atmospheric boundary layer: Effects of dust and sea-salt particles," J. Geophys. Res. **104**(D24), 31781–31792 (1999).
12. Z. Huang, J. Huang, J. Bi, G. Wang, W. Wang, Q. Fu, Z. Li, S.-C. Tsay, and J. Shi, "Dust aerosol vertical structure measurements using three MPL lidars during 2008 China-U.S. joint dust field experiment," J. Geophys. Res. **115**, D00K15 (2010).
13. N. Sugimoto and Z. Huang, "Lidar methods for observing mineral dust," J. Meteorol. Res. **28**(2), 173–184 (2014).
14. N. Sugimoto, Z. Huang, T. Nishizawa, I. Matsui, and B. Tatarov, "Fluorescence from atmospheric aerosols observed with a multi-channel lidar spectrometer," Opt. Express **20**(19), 20800 (2012).
15. Q. Dong, Z. Huang, W. Li, Z. Li, X. Song, W. Liu, T. Wang, J. Bi, and J. Shi, "Polarization Lidar Measurements of Dust Optical Properties at the Junction of the Taklimakan Desert–Tibetan Plateau," Remote Sens. **14**(3), 558 (2022).
16. X. Ma, Z. Huang, S. Qi, J. Huang, S. Zhang, Q. Dong, and X. Wang, "Ten-year global particulate mass concentration derived from space-borne CALIPSO lidar observations," Sci. Total Environ. **721**, 137699 (2020).
17. C. F. Bohren and D. R. Huffman, "*Absorption and Scattering of Light by Small Particles*." (Wiley, 1983).

Optics EXPRESS

18. G. David, B. Thomas, T. Nousiainen, A. Miffre, and P. Rairoux, "Retrieving simulated volcanic, desert dust and sea-salt particle properties from two/three-component particle mixtures using UV-VIS polarization lidar and T matrix," Atmos. Chem. Phys. **13**(14), 6757–6776 (2013).
19. Z. Liu, D. Liu, J. Huang, M. Vaughan, I. Uno, N. Sugimoto, C. Kittaka, C. Trepte, Z. Wang, C. Hostetler, and D. Winker, "Airborne dust distributions over the Tibetan Plateau and surrounding areas derived from the first year of CALIPSO lidar observations," Atmos. Chem. Phys. **8**(16), 5045–5060 (2008).
20. R. E. Mamouri and A. Ansmann, "Fine and coarse dust separation with polarization lidar," Atmos. Meas. Tech. **7**(11), 3717–3735 (2014).
21. Z. Huang, S. Qi, T. Zhou, Q. Dong, and J. Shi, "Investigation of aerosol absorption with dual-polarization lidar observations," Opt. Express **28**(5), 7028 (2020).
22. M. I. Mishchenko and L. D. Travis, "Capabilities and limitations of a current FORTRAN implementation of the T -matrix method for randomly oriented, rotationally symmetric scatterers," J. Quant. Spectrosc. Radiat. Transfer **60**(3), 309–324 (1998).
23. M. I. Mishchenko, J. M. Dlugach, and L. Liu, "Linear depolarization of lidar returns by aged smoke particles," Appl. Opt. **55**(35), 9968 (2016).
24. L. Bi, W. Lin, Z. Wang, X. Tang, X. Zhang, and B. Yi, "Optical Modeling of Sea Salt Aerosols: The Effects of Nonsphericity and Inhomogeneity," J. Geophys. Res.: Atmos. **123**(1), 543–558 (2018).
25. T. Nousiainen, M. Kahnert, and B. Veihelmann, "Light scattering modeling of small feldspar aerosol particles using polyhedral prisms and spheroids," J. Quant. Spectrosc. Radiat. Transfer **101**(3), 471–487 (2006).
26. T. Nousiainen, M. Kahnert, and H. Lindqvist, "Can particle shape information be retrieved from light-scattering observations using spheroidal model particles?" J. Quant. Spectrosc. Radiat. Transfer **112**(13), 2213–2225 (2011).
27. M. Haarig, A. Ansmann, J. Gasteiger, K. Kandler, D. Althausen, H. Baars, M. Radenz, and D. A. Farrell, "Dry versus wet marine particle optical properties: RH dependence of depolarization ratio, backscatter, and extinction from multiwavelength lidar measurements during SALTRACE," Atmos. Chem. Phys. **17**(23), 14199–14217 (2017).
28. Z. Huang, J. B. Nee, C. W. Chiang, S. Zhang, H. Jin, W. Wang, and T. Zhou, "Real-time observations of dust-cloud interactions based on polarization and Raman lidar measurements," Remote Sens. **10**(7), 1017 (2018).
29. W. Sun, Z. Liu, G. Videen, Q. Fu, K. Muinonen, D. M. Winker, C. Lukashin, Z. Jin, B. Lin, and J. Huang, "For the depolarization of linearly polarized light by smoke particles," J. Quant. Spectrosc. Radiat. Transfer **122**, 233–237 (2013).
30. M. I. Mishchenko, L. D. Travis, and A. A. Lacis, "*Scattering, absorption, and emission of light by small particles*," (2002).
31. Z. Liu, "Use of probability distribution functions for discriminating between clouds and aerosol in lidar backscatter data," J. Geophys. Res. **109**(D15), D15202 (2004).
32. B. Liu, Y. Ma, W. Gong, and M. Zhang, "Observations of aerosol color ratio and depolarization ratio over Wuhan," Atmos. Pollut. Res. **8**(6), 1113–1122 (2017).
33. Y. Song, B. Zhang, G. Shi, S. Li, H. Di, Q. Yan, and D. Hua, "Correlation between the lidar ratio and the Ångström exponent of various aerosol types," Particuology **40**, 62–69 (2018).
34. O. Dubovik, A. Sinyuk, T. Lapyonok, B. N. Holben, M. Mishchenko, P. Yang, T. F. Eck, H. Volten, O. Muñoz, B. Veihelmann, W. J. van der Zande, J. F. Leon, M. Sorokin, and I. Slutsker, "Application of spheroid models to account for aerosol particle nonsphericity in remote sensing of desert dust," J. Geophys. Res. **111**(D11), D11208 (2006).
35. J. Gasteiger and V. Freudenthaler, "Benefit of depolarization ratio at = 1064 nm for the retrieval of the aerosol microphysics from lidar measurements," Atmos. Meas. Tech. **7**(11), 3773–3781 (2014).
36. X. Huang, P. Yang, G. Kattawar, and K. N. Liou, "Effect of mineral dust aerosol aspect ratio on polarized reflectance," J. Quant. Spectrosc. Radiat. Transfer **151**, 97–109 (2015).
37. K. Okada, J. Heintzenberg, K. Kai, and Y. Qin, "Shape of atmospheric mineral particles collected in three Chinese arid-regions," Geophys. Res. Lett. **28**(16), 3123–3126 (2001).
38. D. Scheuvens, K. Kandler, M. KüPPER, K. Lieke, S. R. Zorn, M. Ebert, L. Schutz, and S. Weinbruch, "Individual-particle analysis of airborne dust samples collected over Morocco in 2006 during SAMUM 1," Tellus B Chem Phys Meteorol **63**(4), 512–530 (2011).
39. J. Gasteiger, M. Wiegner, S. Gro, V. Freudenthaler, C. Toledano, M. Tesche, and K. Kandler, "Modelling lidar-relevant optical properties of complex mineral dust aerosols," Tellus B Chem Phys Meteorol **63**(4), 725–741 (2011).
40. L. Li, X. Zheng, Z. Li, Z. Li, and M. Wendisch, "Studying aerosol light scattering based on aspect ratio distribution observed by fluorescence microscope," Opt. Express **25**(16), A813 (2017).
41. K. Adachi, S. H. Chung, and P. R. Buseck, "Shapes of soot aerosol particles and implications for their effects on climate," J. Geophys. Res. **115**(D15), D15206 (2010).
42. A. Gialitaki, A. Tsekeri, V. Amiridis, R. Ceolato, and D. Balis, "Is near-spherical shape 'the new black' for smoke?" EPJ Web Conf. **237**(D17201), 02017 (2020).
43. L. Liu and M. I. Mishchenko, "Spectrally dependent linear depolarization and lidar ratios for nonspherical smoke aerosols," J. Quant. Spectrosc. Radiat. Transfer **248**, 106953 (2020).
44. J. Bi, J. Huang, B. Holben, and G. Zhang, "Comparison of key absorption and optical properties between pure and transported anthropogenic dust over East and Central Asia," Atmos. Chem. Phys. **16**(24), 15501–15516 (2016).
45. S. P. Burton, J. W. Hair, M. Kahnert, R. A. Ferrare, C. A. Hostetler, A. L. Cook, D. B. Harper, T. A. Berkoff, S. T. Seaman, J. E. Collins, M. A. Fenn, and R. R. Rogers, "Observations of the spectral dependence of linear particle

Optics EXPRESS

depolarization ratio of aerosols using NASA Langley airborne High Spectral Resolution Lidar," Atmos. Chem. Phys. **15**(23), 13453–13473 (2015).
46. I. S. Zo and S. K. Shin, "A short note on the potential of utilization of spectral AERONET-derived depolarization ratios for aerosol classification," Atmosphere **10**(3), 143 (2019).
47. Y. M. Noh, S. K. Shin, K. Lee, D. Müller, and K. Kim, "Utilization of the depolarization ratio derived by AERONET Sun/sky radiometer data for type confirmation of a mixed aerosol plume over East Asia," Int. J. Remote Sens. **37**(10), 2180–2197 (2016).
48. S. Zhang, Z. Huang, M. Li, X. Shen, Y. Wang, Q. Dong, J. Bi, J. Zhang, W. Li, Z. Li, and X. Song, "Vertical structure of dust aerosols observed by a ground-based raman lidar with polarization capabilities in the center of the Taklimakan desert," Remote Sens. **14**(10), 2461 (2022).
49. L. Bi, W. Lin, D. Liu, and K. Zhang, "Assessing the depolarization capabilities of nonspherical particles in a super-ellipsoidal shape space," Opt. Express **26**(2), 1726 (2018).
50. S. Qi, Z. Huang, X. Ma, J. Huang, T. Zhou, S. Zhang, Q. Dong, J. Bi, and J. Shi, "Classification of atmospheric aerosols and clouds by use of dual-polarization lidar measurements," Opt. Express **29**(15), 23461–23476 (2021).
51. L. Bi, P. Yang, G. W. Kattawar, B. A. Baum, Y. X. Hu, D. M. Winker, R. Scott Brock, and J. Q. Lu, "Simulation of the color ratio associated with the backscattering of radiation by ice particles at the wavelengths of 0.532 and 1.064 μm," J. Geophys. Res. **114**(D4), D00H08 (2009).
52. M. Haarig, A. Ansmann, H. Baars, C. Jimenez, I. Veselovskii, R. Engelmann, and D. Althausen, "Depolarization and lidar ratios at 355, 532, and 1064 nm and microphysical properties of aged tropospheric and stratospheric Canadian wildfire smoke," Atmos. Chem. Phys. **18**(16), 11847–11861 (2018).
53. J. Shen, N. Cao, and Y. Zhao, "Accurate retrieval of aerosol lidar ratio by Raman-Mie lidar in Nanjing," Optik **227**, 165980 (2021).
54. D. Müller, I. Veselovskii, A. Kolgotin, M. Tesche, A. Ansmann, and O. Dubovik, "Vertical profiles of pure dust and mixed smoke-dust plumes inferred from inversion of multiwavelength Raman/polarization lidar data and comparison to AERONET retrievals and in situ observations," Appl. Opt. **52**(14), 3178–3202 (2013).
55. T. Nishizawa, N. Sugimoto, I. Matsui, A. Shimizu, and H. Okamoto, "Algorithms to retrieve optical properties of three component aerosols from two-wavelength backscatter and one-wavelength polarization lidar measurements considering nonsphericity of dust," J. Quant. Spectrosc. Radiat. Transfer **112**(2), 254–267 (2011).
56. S. Bohlmann, X. Shang, V. Vakkari, E. Giannakaki, A. Leskinen, K. E. J. Lehtinen, S. Ptsi, and M. Komppula, "Lidar depolarization ratio of atmospheric pollen at multiple wavelengths," Atmos. Chem. Phys. **21**(9), 7083–7097 (2021).
57. S. Groß, M. Tesche, V. Freudenthaler, C. Toledano, M. Wiegner, A. Ansmann, D. Althausen, and M. Seefeldner, "Characterization of Saharan dust, marine aerosols and mixtures of biomass-burning aerosols and dust by means of multi-wavelength depolarization and Raman lidar measurements during SAMUM 2," Tellus B Chem Phys Meteorol **63**(4), 706–724 (2011).
58. S. Groß, V. Freudenthaler, K. Schepanski, C. Toledano, A. Schäfler, A. Ansmann, and B. Weinzierl, "Optical properties of long-range transported Saharan dust over Barbados as measured by dual-wavelength depolarization Raman lidar measurements," Atmos. Chem. Phys. **15**(19), 11067–11080 (2015).
59. M. Haarig, A. Ansmann, R. Engelmann, H. Baars, D. Althausen, C. Toledano, B. Torres, M. Radenz, and U. Wandinger, "First triple-wavelength lidar observations of depolarization and extinction-to-backscatter ratios of Saharan dust," Atmos. Chem. Phys. **22**(1), 355–369 (2022).